Flow Reactor Studies and Kinetic Modeling of the H_2/O_2 Reaction

M. A. MUELLER, T. J. KIM, R. A. YETTER, F. L. DRYER

Department of Mechanical and Aerospace Engineering, Princeton University, Princeton, New Jersey 08536

Received 10 June 1998; accepted 20 August 1998

ABSTRACT: Profile measurements of the H_2/O_2 reaction have been obtained using a variable pressure flow reactor over pressure and temperature ranges of 0.3–15.7 atm and 850–1040 K, respectively. These data span the explosion limit behavior of the system and place significant emphasis on HO_2 and H_2O_2 kinetics. The explosion limits of dilute $H_2/O_2/N_2$ mixtures extend to higher pressures and temperatures than those previously observed for undiluted H_2/O_2 mixtures. In addition, the explosion limit data exhibit a marked transition to an extended second limit which runs parallel to the second limit criteria calculated by assuming HO_2 formation to be terminating. The experimental data and modeling results show that the extended second limit remains an important boundary in H_2/O_2 kinetics. Near this limit, small increases in pressure can result in more than a two order of magnitude reduction in reaction rate. At conditions above the extended second limit, the reaction is characterized by an overall activation energy much higher than in the chain explosive regime.

The overall data set, consisting primarily of experimentally measured profiles of H_2, O_2, H_2O, and temperature, further expand the data base used for comprehensive mechanism development for the H_2/O_2 and $CO/H_2O/O_2$ systems. Several rate constants recommended in an earlier reaction mechanism have been modified using recently published rate constant data for $H + O_2 (+ N_2) = HO_2 (+ N_2)$, $HO_2 + OH = H_2O + O_2$, and $HO_2 + HO_2 = H_2O_2 + O_2$. When these new rate constants are incorporated into the reaction mechanism, model predictions are in very good agreement with the experimental data. Int J Chem Kinet 31: 113–125, 1999

INTRODUCTION

The hierarchical development of detailed kinetic mechanisms for hydrocarbon oxidation and other complicated reacting systems necessarily begins with the H_2/O_2 chemistry which plays a prominent role in determining the composition of the radical pool [1]. While the kinetics of the H_2/O_2 systems have been extensively studied [2,3], reactions involving the formation and consumption of HO_2 and H_2O_2 are comparatively less understood than the chain-branched reactions which dominate at low pressures and high temperatures. In a previous paper [4], we presented a moist CO oxidation reaction mechanism incorporating a detailed H_2/O_2 submechanism developed and validated using high-pressure (2.5–15.7 atm) flow reactor data which placed significant emphasis on reactions involving HO_2 and H_2O_2 [5]. Since that publication, new rate constant data have been published for several important reactions including $H + O_2 (+M) = HO_2 (+M)$ [6,7] and $HO_2 + OH = H_2O + O_2$ [8]. In particular, the studies of Bromly et al. [6] and Davidson et al. [7] recommended rate expressions for $H + O_2$

Correspondence to: F. L. Dryer
Contract grant sponsor: Department of Energy, Office of Basic Energy Sciences
Contract grant number: SE-FG02-86ER-13503
Contract grant sponsor: Air Force Office of Scientific Research
Contract grant number: F49620-93-1-0427
 CCC 0538-8066/99/020113-13

+ N_2 = HO_2 + N_2 which, when incorporated into our H_2/O_2 submechanism, adversely affected the predictive ability of the $CO/H_2O/O_2$ mechanism at conditions where HO_2/H_2O_2 chemistry is important. To resolve this discrepancy, we recently derived new rate constant data for the low-pressure limit H + O_2 + M = HO_2 + M (M = N_2,Ar) [9]. As discussed here, we also obtained new experimental data on the H_2/O_2 reaction in order to update the H_2/O_2 submechanism in a manner consistent with the new rate constant data as well as the concurrent development of $H_2/O_2/NO_X$ [10], H_2/N_2O [11], and H_2/NO_2 [12] reaction mechanisms. In addition, recent modifications to our experimental facility have extended the operating range of our flow reactor to subatmospheric pressures. This new capability enabled a more complete characterization of the explosion limit behavior of dilute $H_2/O_2/N_2$ mixtures.

The entire data set of the present study spans pressure, temperature, and residence time ranges of 0.3–15.7 atm, 850–1040 K, and 0.03–1.4 sec, respectively. Reaction profiles were obtained at initial conditions within both the chain explosive and thermal/chain explosive regimes of H_2/O_2 chemistry and particular emphasis was placed on exploring the extended second explosion limit which demarcates these two kinetic regimes. In the chain explosive regime between the first and second explosion limits, H_2/O_2 kinetics are largely controlled by the chain-branched sequence

$$H + O_2 = OH + O \quad (1)$$

$$O + H_2 = H + OH \quad (2)$$

$$OH + H_2 = H_2O + H \quad (3)$$

and the overall reaction is characterized by an activation energy approximately equal to that of the rate-limiting reaction H + O_2 = OH + O [13]. In the thermal/chain explosive regime above the extended second limit, H atoms are primarily consumed through the termolecular reaction

$$H + O_2(+M) = HO_2(+M). \quad (9)$$

At conditions where the relatively unreactive HO_2 radicals do not undergo further reaction or are destroyed at vessel walls, reaction (9) is chain terminating and a steady-state analysis of the radical pool gives the analytical expression $2k_1 = k_{9,\mathrm{eff}}$ commonly associated with the second limit. However, as shown by Baldwin and co-workers [14–18], the consideration of gas-phase consumption of HO_2 radicals is necessary to predict explosion limit behavior when heterogeneous radical destruction is suppressed. In this case, HO_2 consumption, primarily through HO_2 + H = OH + OH or HO_2 + HO_2 = H_2O_2 + O_2 followed by H_2O_2 (+M) = OH + OH (+M), propagates chain carriers.

REACTION MECHANISM

The updated H_2/O_2 reaction mechanism consists of the 19 reversible elementary reactions and thermochemical data listed in Tables I and II, respectively. Reverse rate constants are computed from the forward rate constants and the equilibrium constants. The thermochemical data for each species considered in the mechanism are from Kee et al. [19] with the exception of the heat of formation for HO_2 which is from Hills and Howard [20].

The reaction mechanism given in Table I is a revision of the H_2/O_2 submechanism of Kim et al. [4] which is itself a revision of the comprehensive $CO/H_2O/O_2$ reaction mechanism of Yetter et al. [21]. The high-pressure flow reactor experiments of Kim [5] were used to refine the rate constants of several reactions involving adducts as well as to incorporate high-pressure fall-off in reactions (9) and (15). The revised rate constants were literature values with the exception of that for HO_2 + OH = H_2O + O_2 which was estimated by fitting available rate data. While our earlier reaction mechanism accurately predicts the H_2/O_2 reaction over a wide range of conditions, recent studies have refined the rate constant data for several elementary reactions involving the formation and consumption of HO_2. These new data have been incorporated into the updated reaction mechanism as follows.

H + O_2(+M) = HO_2(+M)

Although much effort has been made to determine the rate constant for this reaction, there remains considerable scatter in the available data for the low-pressure limit, $k_{9,0}$, and only the study of Cobos et al. [22] has investigated the high-pressure limit, $k_{9,\infty}$. In a recent study [9], we obtained new rate constant data for $k_{9,0}^{N_2}$ at temperatures ranging from 800–900 K and utilized previously reported data to derive a low-pressure limit of $k_{9,0}^{N_2} = 3.5 \times 10^{16}\, T^{-0.41}\exp(+1116/RT)$ cm^6 $mole^{-2}$ sec^{-1} over the temperature range 300–1600 K. While the difference between this expression and the low-pressure limit of Slack [23] used in our earlier mechanisms is small over the temperature range of 800–1200 K, we now determine high-pressure fall-off using the Troe formulation [24] with the broad-

Table I H_2/O_2 Reaction Mechanism. Units Are cm^3-mole-sec-kcal-K; $k = AT^n \exp(-E_a/RT)$

	ΔH°_{298}		A	n	E_a	Reference
H_2/O_2 Chain Reactions						
1. $H + O_2 = O + OH$	16.77		1.91×10^{14}	0.00	16.44	Pirraglia et al. [25]
2. $O + H_2 = H + OH$	1.85		5.08×10^{4}	2.67	6.29	Sutherland et al [55]
3. $H_2 + OH = H_2O + H$	−15.01		2.16×10^{8}	1.51	3.43	Michael et al. [56]
4. $O + H_2O = OH + OH$	16.88		2.97×10^{6}	2.02	13.4	Sutherland et al. [57]
H_2/O_2 Dissociation/Recombination Reactions						
5. $H_2 + M = H + H + M$[a]	104.2		4.58×10^{19}	−1.40	104.38	Tsang et al. [39]
$H_2 + Ar = H + H + Ar$	104.2		5.84×10^{18}	−1.10	104.38	Tsang et al. [39]
6. $O + O + M = O_2 + M$[a]	−119.1		6.16×10^{15}	−0.50	0.00	Tsang et al. [39]
$O + O + Ar = O_2 + Ar$	−119.1		1.89×10^{13}	0.00	−1.79	Tsang et al. [39]
7. $O + H + M = OH + M$[a]	−102.3		4.71×10^{18}	−1.0	0.00	Tsang et al. [39]
8. $H + OH + M = H_2O + M$[a]	−119.2		2.21×10^{22}	−2.00	0.00	Tsang et al. [39]
$H + OH + Ar = H_2O + Ar$	−119.2		8.41×10^{21}	−2.00	0.00	Tsang et al. [39]
Formation and Consumption of HO_2						
9. $H + O_2 + M = HO_2 + M$[a]	−49.1	k_O	3.5×10^{16}	−0.41	−1.12	Mueller et al. [9]
$H + O_2 + Ar = HO_2 + Ar$	−49.1	k_O	1.5×10^{15}	0.00	−1.00	Baulch et al. [60]
$H + O_2 = HO_2$[c]		k_∞	1.48×10^{12}	0.60	0.00	Cobos et al. [22]
10. $HO_2 + H = H_2 + O_2$	55.1		1.66×10^{13}	0.00	0.82	see text
11. $HO_2 + H = OH + OH$	−36.47		7.08×10^{13}	0.00	0.30	see text
12. $HO_2 + O = OH + O_2$	−52.23		3.25×10^{13}	0.00	0.00	Baulch et al. [30]
13. $HO_2 + OH = H_2O + O_2$	−70.11		2.89×10^{13}	0.00	−0.50	Baulch et al. [30]
Formation and Consumption of H_2O_2						
14. $HO_2 + HO_2 = H_2O_2 + O_2$[b]	−38.53		4.20×10^{14}	0.00	11.98	Hippler et al. [40]
$HO_2 + HO_2 = H_2O_2 + O_2$[b]			1.30×10^{11}	0.00	−1.63	
15. $H_2O_2 + M = OH + OH + M$[a]	−51.14	k_O	1.20×10^{17}	0.00	45.5	Warnatz [58]
$H_2O_2 + Ar = OH + OH + Ar$	−51.14	k_O	1.90×10^{16}	0.00	43.0	Brouwer et al. [59]
$H_2O_2 = OH + OH$[c]		k_∞	2.95×10^{14}	0.00	48.4	Brouwer et al. [59]
16. $H_2O_2 + H = H_2O + OH$	−68.05		2.41×10^{13}	0.00	3.97	Tsang et al. [39]
17. $H_2O_2 + H = H_2 + HO_2$	−16.57		4.82×10^{13}	0.00	7.95	Tsang et al. [39]
18. $H_2O_2 + O = OH + HO_2$	−14.70		9.55×10^{6}	2.00	3.97	Tsang et al. [39]
19. $H_2O_2 + OH = H_2O + HO_2$[b]	−31.58		1.00×10^{12}	0.00	0.00	Hippler et al. [34]
$H_2O_2 + OH = H_2O + HO_2$[b]			5.8×10^{14}	0.00	9.56	

[a] Efficiency factors for the collision partners of this pressure dependent reaction are: $\epsilon_{H_2O} = 12.0$; $\epsilon_{H_2} = 2.5$; and $\epsilon_{Ar} = 0.75$. All other species have efficiencies equal to unity. When a rate constant is declared specifically for an Argon collision partner, the efficiency of Argon is set to zero when determining M for the same reaction.

[b] Reactions 14 and 19 are expressed as the sum of the two rate expressions.

[c] Reaction 9 is given as a true fit with $F_c^{N_2} = 0.5$ and $F_c^{Ar} = 0.45$. Reaction 15 is given as a true fit with $F_c = 0.5$.

Table II $\Delta H_f(298.15)$, S(298.15), and c_p (T) for Species Considered in the H_2/O_2 Reaction Mechanism. Units Are cal. $mole^{-1}$ deg^{-1} for c_p and S and kcal $mole^{-1}$ for ΔH_f

Species	$\Delta H_f(298.15)$	$S(298.15)$	$c_p(300)$	$c_p(500)$	$c_p(800)$	$c_p(1000)$	$c_p(1500)$	$c_p(2000)$
H	52.103 ± 0.001	27.416 ± 0.004	4.97	4.97	4.97	4.97	4.97	4.97
O	59.55 ± 0.024	38.49 ± 0.005	5.23	5.08	5.02	5.00	4.98	4.98
OH	9.318 ± 0.29	43.905 ± 0.01	7.15	7.07	7.13	7.33	7.87	8.28
H_2	0.0	31.232 ± 0.008	6.90	7.00	7.07	7.21	7.73	8.18
O_2	0.0	49.03 ± 0.008	7.01	7.44	8.07	8.35	8.72	9.03
H_2O	−57.795 ± 0.01	45.13 ± 0.01	8.00	8.45	9.22	9.87	11.26	12.22
HO_2	3.0 ± 0.4	54.75 ± 0.02	8.34	9.49	10.78	11.39	12.45	13.22
H_2O_2	−32.53	55.66	10.42	12.35	14.29	15.21	16.85	17.88
N_2	0.0	45.93 ± 0.005	6.95	7.08	7.50	7.83	8.32	8.60
Ar	0.0	37.00 ± 0.001	4.97	4.97	4.97	4.97	4.97	4.97

ening factor $F_C^{N_2} = 0.5$ recommended by Cobos et al. [22] instead of the Lindemann fit used previously. As a result, the new pressure-dependent expression yields values for $k_{9,eff}^{N_2}$ which are approximately 20–30% lower at the conditions of the present study. As will be shown in a later figure, the use of $k_{9,eff}^{N_2}$ with appropriate chaperone efficiencies and the k_1 recommendation of Pirraglia et al. [25] results in very good agreement with H_2/O_2 explosion limit data over the temperature range 675–900 K. We note that the expression of Pirraglia et al. overpredicts recent data [26–29] for H + O_2 = OH + O at temperatures in excess of 1700 K. However, extrapolation of recent k_1 recommendations [30] to temperatures below 1000 K yields values which are significantly higher than those supported by combined ($k_1 + k_{9,0}^{Ar}$[Ar]) rate data obtained between 746–987 K [25]. This discrepancy suggests that a non-Arrhenius temperature dependency may be required to best represent k_1 over the entire temperature range spanning 700–5300 K. We continue to use the recommendation of Pirraglia et al. below 1700 K and recommend additional studies to better characterize k_1 at temperatures below 1000 K.

$HO_2 + OH = H_2O + O_2$

The reaction of HO_2 with OH competes with reaction (11) for HO_2 radicals and, in doing so, inhibits the overall reaction rate. Due to its importance in the HO_X cycle of atmospheric chemistry, this reaction has been extensively studied and is well-characterized at low temperatures [31–33]. The high-temperature data [34] used to develop the expression for k_{13} in our earlier mechanism have been refined and additional data, shown in Figure 1, have been obtained by Hippler et al. [35] over the temperature range 1100–1600 K. This new data exhibits a highly non-Arrhenius temperature dependency indicative of the formation of an activated complex. While a complete description of this complex reaction requires more data over larger ranges of pressure and temperature, it is likely that our previous expression for k_{13} is too low at temperatures less than 1000 K. We therefore accept the recommendation of Baulch et al. [30] which is based upon the low-temperature work of Keyser [31]. This expression does not capture the anomalous temperature dependency exhibited by the experimental data; however, at temperatures in excess of 1100 K, reaction (13) is of minor importance except at high pressures and fuel-lean conditions.

$HO_2 + H = OH + OH$; $HO_2 + H = H_2 + O_2$

Rate data and product ratios for the competing reactions $HO_2 + H = OH + OH$ and $HO_2 + H = H_2 +$

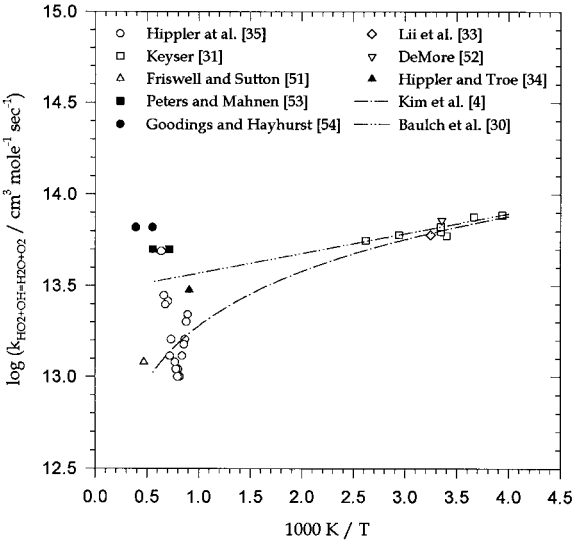

Figure 1 Arrhenius plot of rate coefficient data for the $HO_2 + OH = H_2O + O_2$ reaction.

O_2 are rather sparse, particularly at temperatures of interest for combustion chemistry. Room-temperature data [36,37] and modeling studies of H_2/O_2 explosion limit data in boric acid-coated vessels [18] and laminar flame speeds of rich $H_2/O_2/N_2$ mixtures [38] indicate that reaction (11) is the dominant reaction pathway. The rate constants for reactions (10) and (11) used in our earlier mechanisms were from Tsang and Hampson [39] who based their recommendation upon the low temperature data of Sridharan et al. [37] and the modeling results of Baldwin et al. [18].

The rate constant data of Baldwin et al. [18], expressed in the form of optimized values for the parameters $k_{11}/k_1k_{14}^{1/2}$ and $k_{10}/k_1k_{14}^{1/2}$ at 773 K, have been updated to incorporate the k_{14} recommendation of Hippler et al. [40]. Furthermore, in order to provide a self-consistent set of rate constants, we use the k_1 expression of Pirraglia et al. [25] rather than the expression used in the original study. The resulting rate constant data at 773 K are combined with the room-temperature data of Keyser [36] and Sridharan et al. [37] to derive the rate constants provided in Table I. These modified rate constants are approximately 40% lower at 773 K than those recommended by Tsang and Hampson [39].

We note that the reaction between HO_2 radicals and H atoms has a third possible product route, $HO_2 + H = H_2O + O$, which is kinetically similar to reaction (11). The data of Keyser [36] and Sridharan et al. [37] as well as the modeling results of Day et al. [38] indicate that this reaction is much slower than reaction (11). Given the large uncertainty in its rate constant,

we do not include $HO_2 + H = H_2O + O$ in our mechanism.

FLOW REACTOR EXPERIMENT

A schematic of the variable pressure flow reactor (VPFR) used in this study is shown in Figure 2. The entire reactor is enclosed in a carbon steel pressure vessel rated for operation from full vacuum to 30 atm. Reactor pressures in excess of one atmosphere are achieved by means of a back-pressure valve located within the reactor exhaust duct. Subatmospheric operation is achieved by replacing this valve with a gas jet compressor which pulls a partial vacuum on the entire pressure vessel.

Carrier gas (typically N_2) is heated by a combined ferrous alloy/tungsten electrical resistance heater and mixed with oxygen as it enters a 10.16 cm diameter quartz tube. The carrier gas/oxygen mixture flows around a 8.9 cm baffle plate into a 0.64 cm gap serving as the entrance to a silica foam diffuser with a 5 degree half angle (Figure 3). The hydrogen is diluted with inert and injected radially outward into this gap where it rapidly mixes with the carrier gas and oxygen. The reacting mixture then flows through the diffuser and into the test section where a hot-water cooled, stainless steel sampling probe continuously extracts and convectively quenches a small percentage of the flow. The sample gas flows via heated teflon lines to a series analytical equipment including a Fourier transform infrared spectrometer (Nicolet Model 730), an electrochemical O_2 analyzer (Infrared Industries Model 2200), and a selective thermal conductivity detector used to measure H_2. The measurement uncertainties for data reported here are: H_2O, $\pm 10\%$; O_2, $\pm 2\%$; and H_2, $\pm 5\%$ of reading. The temperature of the reacting mixture is measured at the sampling location with a silica-coated type R thermocouple accurate to approximately ± 3 K [41].

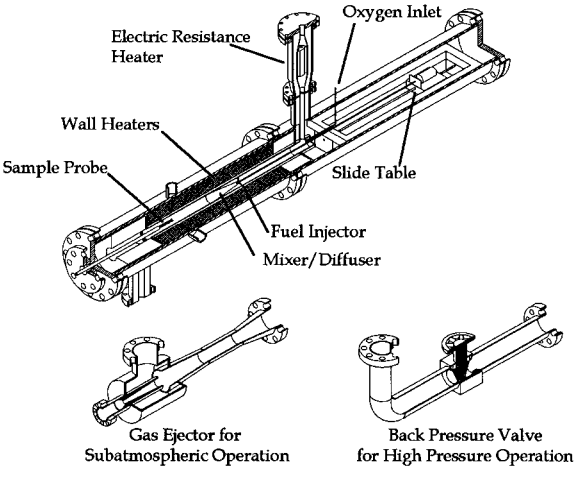

Figure 2 Schematic of the variable pressure flow reactor with the gas ejector and back pressure valve which enable operation at subatmospheric and superatmospheric pressures, respectively.

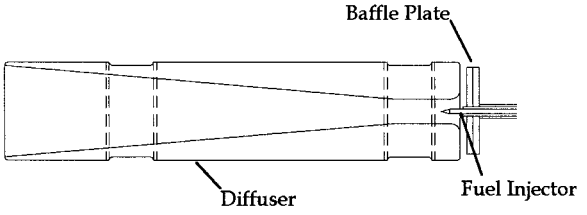

Figure 3 Schematic of the fuel injector/mixer/diffuser assembly.

The distance between the point of fuel injection and sampling location is varied by moving the injector and mixer/diffuser assembly relative to the fixed sampling location by means of a computer-controlled stepper motor. Mean velocity measurements along the centerline of the reactor have been used to correlate distance with residence time and experimental conditions are chosen to produce reaction zones in which a centimeter of distance corresponds to as little as 10^{-4} to 10^{-2} seconds of reaction time. The dilute nature of the $H_2/O_2/N_2$ mixtures used in this study ensures that the maximum temperature rise due to reaction is only a small percentage (2–10%) of the initial gas temperature. Five individually controlled electric resistance heaters maintain the local wall temperature of the quartz tube at the initial gas temperature, thereby approximating an adiabatic reaction zone.

In the vicinity of the injection point, mixing and diffusive effects are non-negligible and influence the chemical induction time. High convective velocities in the downstream test section are used to suppress spatial gradients and, in general, permit neglect of the diffusive terms in the governing equations. The experimental test section can therefore be modeled as a zero-dimensional system using SENKIN [42] with isobaric and adiabatic assumptions provided that there is no memory effect of the chemical perturbations in the mixing region. In an earlier paper [21], we have shown that for the $CO/H_2O/O_2$ system, such perturbations affect the chemical induction times and not the reaction gradients in the test section. Similar analyses of the H_2/O_2 system at the conditions used within the present study have confirmed the same behavior and, for comparative purposes, model predictions are shifted in time to agree with the experimental data at

the point of 50% fuel consumption. Under certain experimental conditions where the characteristic time of the reaction becomes very short, large spatial gradients cannot be avoided. In these instances, the assumption of negligible axial diffusion is exacerbated and comparisons between experimental data and model predictions generated using the zero-dimensional approximation must be regarded with caution. We include comments to this effect in the figure captions of the experimental data and model predictions for which this cautionary note applies.

EXPERIMENTAL RESULTS AND DISCUSSION

An example of experimental data (symbols) and modeling results (lines) obtained in this study is provided in Figure 4. The pressure (3.02 atm) and initial temperature (934 K) chosen for this experiment are within the thermal/chain explosive regime above the explosion limit. The ensuing reaction begins slowly but accelerates as heat release increases the mixture temperature. When the reaction is approximately 25 percent complete, a critical state is reached, at which point the reaction rapidly accelerates and quickly consumes the remaining reactants. The transition to explosively-fast, chain-branched chemistry occurs when the temperature crosses the extended second limit, thereby establishing an overall branching factor in excess of the critical value.

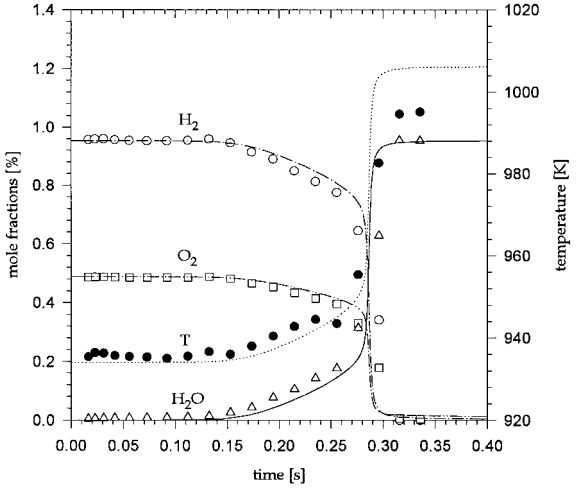

Figure 4 Reaction profiles for the H_2/O_2 reaction at 3.02 atm and T_{in} = 934 K. Symbols represent experimental data; lines represent model predictions. Initial mole fractions are listed in the Appendix. The zero-dimensional assumption may not be valid during the rapid portion of the reaction.

The agreement between the experimental data and model predictions shown in Figure 4 is very good with the exception that the model predicts a more abrupt transition than is observed experimentally. We also note that the measured temperature rise is approximately 10 K lower than that predicted using the adiabatic assumption. This latter discrepancy can be decreased by incorporating a zero-dimensional heat loss term, $q_{LOSS} = h(T - T_{WALL})$, into the energy equation solved within SENKIN. In this manner, the global heat transfer coefficient, h, can be adjusted to improve agreement between the predicted and measured peak temperatures. However, the inclusion of this heat loss term results in only slight changes in the predicted species profiles and, rather than introduce further complexity into the model, we use the adiabatic approximation to generate the model predictions presented in Figure 4 as well as in subsequent figures.

The change in H_2/O_2 kinetics upon crossing the extended second limit is further illustrated in Figure 5 which shows experimental data obtained at three different pressures. The initial mixture temperature in each of these experiments was approximately 935 K. At 2.55 atm, the mixture is within the chain explosive regime and, after a short induction period, a very rapid reaction completely consumes the reactants within a few milliseconds. Increasing the pressure to 3.44 atm moves the initial conditions into the thermal/chain regime and the subsequent reduction in the overall branching factor results in a much slower reaction. However, as before, the heat release of this slow reaction is sufficient to bring the mixture to an explosive condition. When the pressure is increased further to 6.00 atm, the heat release is no longer sufficient to move to the mixture temperature into the chain explosive regime and the reactants are consumed in a slow, steady reaction.

Transitional chemistry of the nature shown in Figures 4 and 5(b) has been observed in the VPFR at pressures ranging from 3.0 to 6.5 atm and provide direct measurements of the extended second limit. At higher pressures, the rate of reaction in the thermal/chain regime increases and, as shown in Figure 6, the transition upon crossing the explosion limit becomes less pronounced and therefore difficult to observe experimentally. Conversely, at pressures lower than 3.0 atm, the reaction in the thermal/chain regime proceeds so slowly as to be unobservable within the timescales of our experiments. Under these circumstances, profile measurements are unable to adequately resolve the transition from slow to fast chemistry. However, near the explosion limit, the overall reaction rate becomes extremely sensitive to small variations in temperature and, as observed in our experiments, the extent of re-

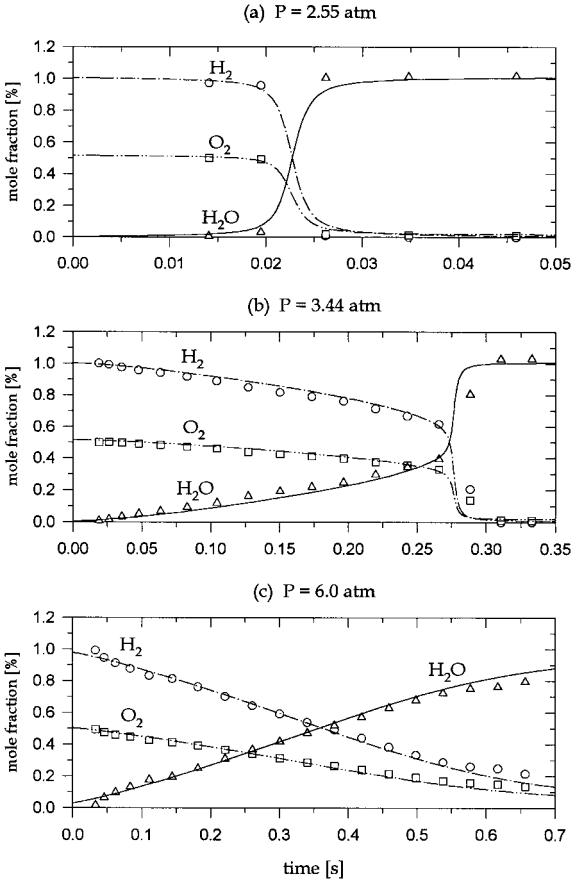

Figure 5 Reaction profiles of the H_2/O_2 reaction at: (a) $P = 2.55$ atm, $T_{in} = 935$ K; (b) $P = 3.44$ atm, $T_{in} = 933$ K; and (c) $P = 6.0$ atm, $T_{in} = 934$ K. Symbols represent experimental data; lines represent model predictions. Initial mole fractions are listed in the Appendix. The zero-dimensional assumption may not be valid for the reaction at 2.55 atm and during the rapid portion of the reaction at 3.44 atm.

action can be changed from zero to 100 percent by increasing the initial temperature by only a few degrees. Explosion limit data from 0.4 to 2.5 atm could therefore be ascertained by gradually increasing the initial mixture temperature until a reaction was observed upon injection of the hydrogen into the carrier gas.

The explosion limit data shown in Figure 7 were obtained using 1.0% H_2/0.5% O_2/N_2 mixtures and represent the minimum temperature at which explosively fast chemistry was observed at the corresponding pressure. Also included in this figure are explosion limit data from several static reactor experiments. These latter data have been modified to take into account the third body efficiencies of H_2 and O_2 relative to N_2. The error bars provided for our data are indicative of the reproducibility of our experimental results.

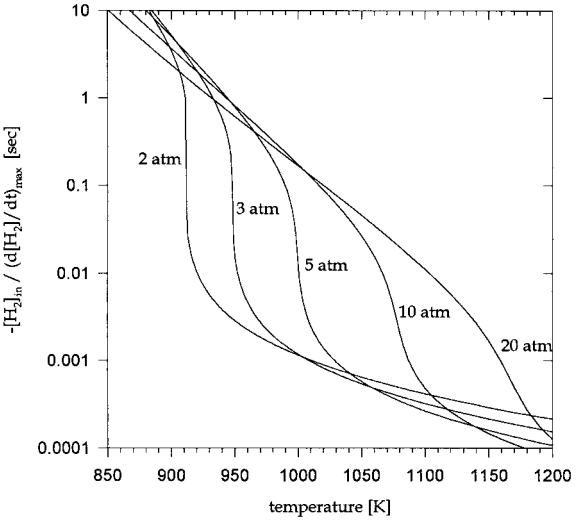

Figure 6 Characteristic reaction times as a function of temperature for dilute $H_2/O_2/N_2$ mixtures at various pressures. Maximum rates of reaction are determined using SENKIN [38] with constant pressure and temperature assumptions. Initial mole fractions are 1.0% H_2, 0.5% O_2, and 98.5% N_2.

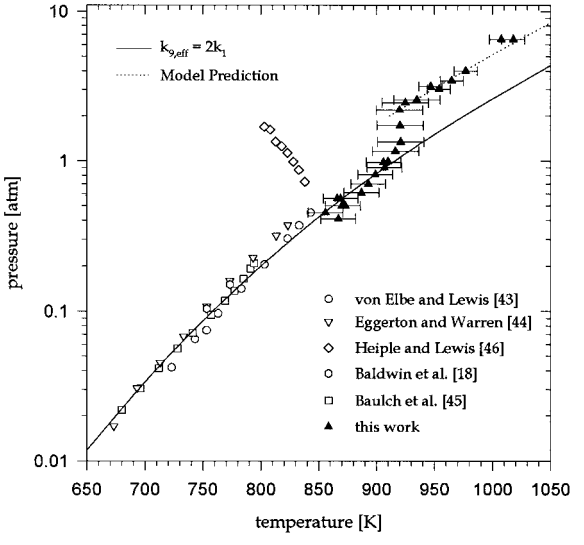

Figure 7 Explosion limit data for stoichiometric H_2/O_2 mixtures as observed in static reactor (○ ▽ ◇ ○), well-stirred reactor (□), and flow reactor (▲) experiments. The data from references [43–46] were obtained using undiluted H_2/O_2 mixtures, those of Baldwin et al. [17] with mixtures of 28% H_2, 14% O_2, and 58% N_2, and those of the present study with mixtures of 1% H_2, 0.5% O_2, and 98.5% N_2. Relative third body efficiencies (ε_{H2}: ε_{N2}: ε_{O2} = 1.0: 0.43: 0.40) are taken from von Elbe and Lewis [43] and are incorporated into pressures as follows: $p = RT[M] \Sigma_i \chi_i \varepsilon_i$. Model predictions ($M = N_2$) are generated using plots similar to those in Figure 6.

As seen in Figure 7, the VPFR data extend well beyond the cusp formed by the convergence of the second and third limits observed in static reactor experiments. At low pressures, the data are in good agreement with the classical second limit criteria of $2k_1 = k_{9,\text{eff}}$. With increasing pressure, the VPFR data digress from this limit; however, rather than fold back to form a third explosion limit, the data shift to an extended second limit which runs parallel to the classical second limit. These unique characteristics can be explained by considering experimental timescales and mixture dilution effects. The relatively long timescales of static reactor experiments allow the observation of reactions with characteristic times much longer than the residence times of reasonable flow reactor experiments. In an adiabatic system, the heat release from these slow reactions can bring the mixture to an explosion condition far removed from the initial conditions. The use of undiluted H_2/O_2 mixtures intensifies self-heating effects and, as noted in several studies, can impose a large thermal influence upon the experimental data in the vicinity of the third limit [46–48]. In fact, the data of Heiple and Lewis [46] are the initial pressures and temperatures for which stoichiometric H_2/O_2 mixtures eventually reached an explosive condition and do not represent the actual conditions at which the chemistry became explosively fast. In contrast, the dilute mixtures used in this study limit self-heating and allow the investigation H_2/O_2 kinetics within narrow temperature ranges. As such, our high-pressure data are more indicative of the kinetic changes that occur when crossing the explosion limit.

The departure of the explosion limit data from the classical second limit occurs when HO_2 consumption via gas-phase reactions begins to propagate the radical pool. As shown in Figure 7, model predictions based solely upon gas-phase kinetics are in excellent agreement with the experimental data along the extended second limit. The accurate prediction of data along the classical second limit requires the development of a mathematical model with both the spatial and temporal dependence necessary to describe the removal of HO_2 radicals by heterogeneous surface kinetics or mass transport (see for example [49,50]). At low pressures, we attribute the loss of chain carriers to heterogeneous reactions or convective losses in which HO_2 acts as a radical sink. The importance of these loss mechanisms is system dependent and, as a result, the location (i.e., pressure and temperature) of the shift in our explosion limit data is unique to the design and operating characteristics of the VPFR. Nonetheless, the experimental data clearly indicate that when HO_2 becomes part of a propagating route, the explosion criteria shifts to lower temperatures than those predicted by the classical second limit criteria. Furthermore, the H_2/O_2 mechanism described in Tables I and II accurately predicts explosion limit behavior at conditions dominated by gas-phase kinetics.

Reaction profile measurements at subatmospheric pressures were obtained at initial conditions within the chain explosive regime where radical losses via heterogeneous wall reactions are negligibly small. Fuel-lean mixtures with initial hydrogen mole fractions of 0.5% were used to limit peak radical concentrations, thereby reducing experimental uncertainty due to diffusive phenomena and recombination reactions within the sampling probe. Figure 8 presents reaction profile data obtained at 0.3 atm with $T_{\text{in}} = 880$ K and an equivalence ratio of 0.5. Model predictions are in excellent agreement with the experimental data and indicate that the radical pool is largely dominated by H atoms. Because the reaction proceeds in the high-temperature regime where $k_1 > k_{9,\text{eff}}$, the largest sensitivity coefficients are associated with the chain-branched sequence consisting of $H + O_2 = OH + O$, $O + H_2 = OH + H$, and $OH + H_2 = H_2O + H$ (Figure 9). However, the formation and consumption of HO_2 remains an important reaction pathway for radical species. H atoms are primarily produced through $OH + H_2 = H_2O + H$ and are consumed via

$$H + O_2(+M) = HO_2(+M) \quad (44.5\%) \qquad (9)$$

$$HO_2 + H = OH + OH \quad (33.8\%) \qquad (11)$$

$$H + O_2 = OH + O \quad (15.7\%) \qquad (1)$$

$$HO_2 + H = H_2 + O_2 \quad (5.9\%) \qquad (10)$$

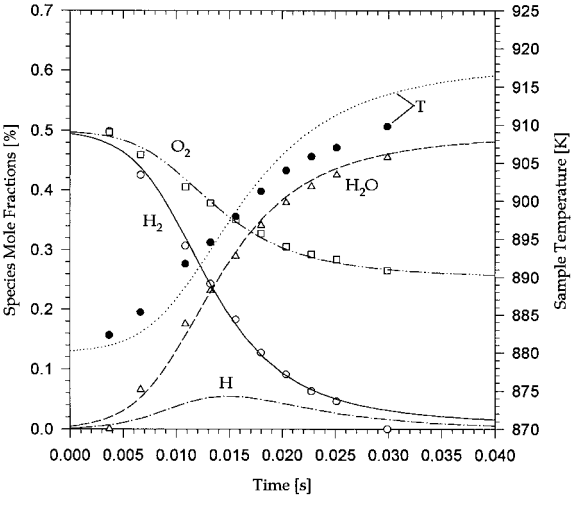

Figure 8 Reaction profiles of the H_2/O_2 reaction at 0.3 atm and $T_{\text{in}} = 880$ K. Symbols represent experimental data; lines represent model predictions. Initial mole fractions are given in the Appendix.

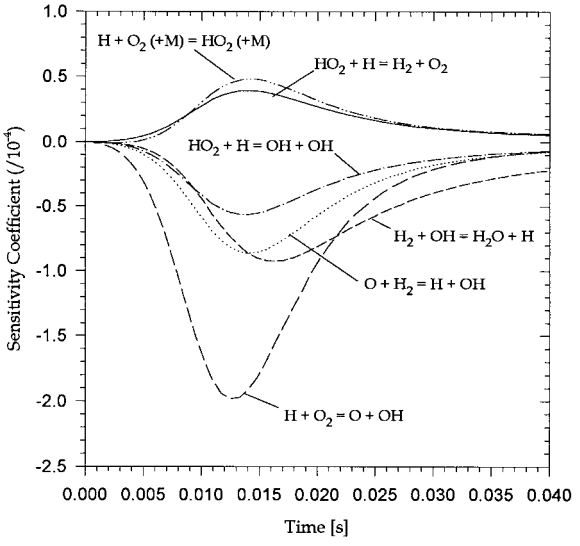

Figure 9 Normalized sensitivity coefficients ($S_{ij} = \partial \ln Y_i / \partial \ln K_j$) for the H_2 mole fraction profile shown in Figure 8.

where the numbers in the second column represent the percentage of H atoms consumed by the corresponding reaction. Due to partial equilibration of reaction (1), reaction (9) becomes the largest consumption route for H atoms even though $k_1 > k_{9,\text{eff}}$. Hydroperoxyl radicals are rapidly consumed via reaction (11) thereby forming a straight-chain sequence, consisting of reactions (9), (11), and (3), which competes with the chain-branched sequence.

In the chain explosive regime, reactions (10) and (11) are the dominant consumption routes for HO_2. For the 0.3 atm experiment discussed here, these reactions consume over 90% of the HO_2 with reaction (11) alone accounting for 77% of the total flux. With increasing pressure, H atom concentrations are suppressed and alternative consumption routes become increasingly active. The importance of these other reaction pathways becomes evident when studying the kinetic response of the H_2/O_2 reaction to changes in stoichiometry. The addition of excess oxygen heightens the role of O and OH radicals as chain carriers and consequently increases the flux of HO_2 through

$$HO_2 + O = O_2 + OH \qquad (12)$$

$$HO_2 + OH = H_2O + O_2. \qquad (13)$$

The degree to which these terminating reactions inhibit the overall reaction depends upon the concentrations of O and OH radicals relative to those of H and HO_2.

The effect of oxygen addition was experimentally investigated at pressures ranging from 0.6 to 15.7 atm. Experimental data and model predictions for three sets of these experiments are presented in Figure 10. The initial conditions at 0.6 atm are within the chain explosive regime, those at 15.7 atm are within the thermal/chain regime, and those at 2.55 atm are in close proximity to the extended second limit. In each case, the addition of excess oxygen increases the ratios [O]/[H] and [OH]/[H]; however, inhibition of the overall reaction rate is only observed at 2.55 atm. As shown in Table III, H atoms are the predominant radical species at 0.6 atm for both equivalence ratios. As a result, the flux of HO_2 through reactions (12) and (13) increases only slightly with the additional oxygen. Reaction (11) remains the primary consumption route for HO_2 and the small inhibiting effect accordant with the increased flux through reactions (12) and (13) is more than offset by the acceleration of reactions (1)

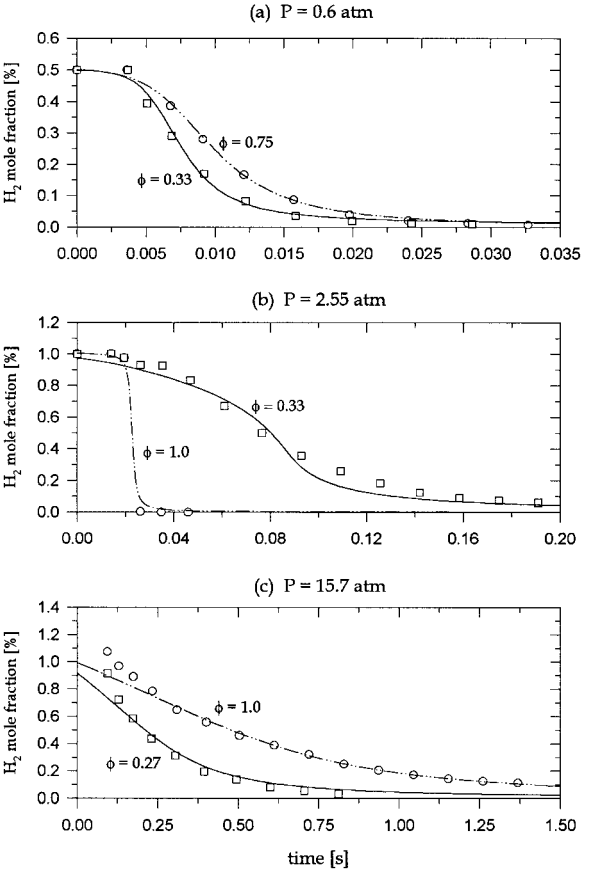

Figure 10 Reaction profiles for stoichiometric and fuel-lean $H_2/O_2/N_2$ mixtures at (a) $P = 0.6$ atm, $T_{in} \cong 897$ K; (b) $P = 2.55$ atm, $T_{in} \cong 940$ K; and (c) $P = 15.7$ atm, $T_{in} = 914$ K. Symbols represent experimental data; lines represent model predictions. Exact initial conditions are listed in the Appendix. The zero-dimensional assumption may not be valid for the stoichiometric reaction at 2.55 atm.

Table III Predicted Composition of Radical Pool for the Experiments Shown in Figure 10. Species Mole Fractions Are Those at the Maximum Rate of Reaction and Are Given in ppm

	P = 0.6 atm		P = 2.55 atm		P = 15.7 atm	
Species	ϕ = 0.75	ϕ = 0.33	ϕ = 1.0	ϕ = 0.33	ϕ = 1.0	ϕ = 0.27
H	318	215	127	6.3	0.02	0.01
O	27.2	39.1	10.9	2.7	0.002	0.004
OH	18.5	29.7	13.0	3.0	0.006	0.01
HO_2	0.9	2.3	3.8	11.4	4.4	6.4
H_2O_2	0.02	0.08	0.1	3.6	12.4	22.6

and (9) which are part of the chain-branched and straight-chain sequences characteristic of the chain explosive regime.

In the vicinity of the extended second limit, the composition of the radical pool is highly sensitive to mixture stoichiometry. In particular, the reduction in equivalence ratio from 1.0 to 0.33 at 2.55 atm reduces the H atom mole fraction by a factor of 20. The O and OH mole fractions are also reduced, but to a much lesser extent, and HO_2 becomes the most abundant radical species. Because the mole fractions of H, O, and OH are of the same order of magnitude at the fuel-lean condition, reactions (12) and (13) can compete effectively with reaction (11). Flux analyses of these experiments are shown in Figure 11 and indicate that the consumption of HO_2 via reactions (12) and (13) increases from 9% to 26% of the total flux upon addition of the excess O_2. In addition, H_2O_2 formation

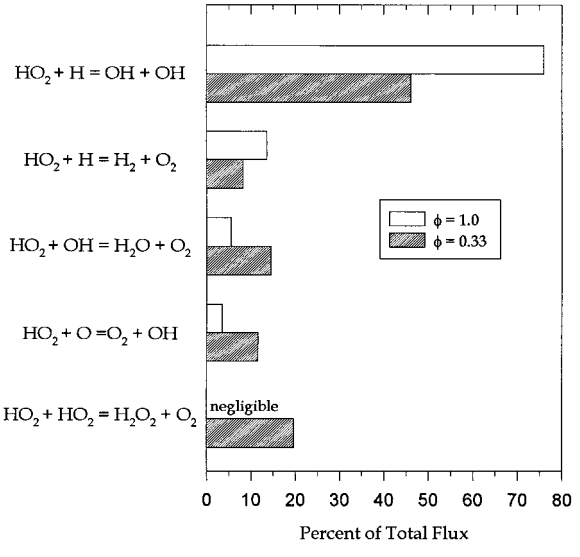

Figure 11 Reaction flux analyses of the consumption of HO_2 in the stoichiometric and lean H_2/O_2 reactions at 2.55 atm shown in Figure 10.

via $HO_2 + HO_2 = H_2O_2 + O_2$, while negligibly small for the stoichiometric reaction, accounts for 20% of the total flux when $\phi = 0.33$. At high pressures and temperatures, the primary consumption route of H_2O_2 is through thermal decomposition; however, at 2.55 atm there are sufficient H, O, and OH radicals to consume approximately 50% of the H_2O_2 via reactions (16–19). These reaction pathways effectively decrease chain propagation and, when combined with the increased flux of HO_2 through reactions (12) and (13), significantly slow the overall reaction rate.

At 15.7 atm, the addition of excess oxygen only slightly alters the radical pool and the HO_2 and H_2O_2 mole fractions are several orders of magnitude larger than those of H, O, and OH. At both equivalence ratios, the consumption of HO_2 is overwhelmingly through $HO_2 + HO_2 = H_2O_2 + O_2$. Due to the high pressure, hydrogen peroxide quickly dissociates via $H_2O_2 (+M) = OH + OH (+M)$ and thereby propagates the radical pool through a straight-chain sequence consisting of reactions (9), (14), (15), and (3). Under these circumstances, the additional oxygen accelerates the overall reaction by accelerating HO_2 production via reaction (9).

The kinetic response to changes in pressure and stoichiometry are summarized in Figure 12 in which the characteristic reaction rates of stoichiometric and fuel-lean $H_2/O_2/N_2$ mixtures at an initial temperature of 935 K are plotted as a function of pressure. At conditions somewhat removed from the extended second limit, increases in pressure increase the rate of reaction. However, as the second limit is crossed, the reduction in chain branching reduces the overall reaction rate by over two orders of magnitude. The addition of excess oxygen inhibits the overall reaction only in the vicinity of the extended second limit and, at conditions within the thermal/chain explosive and chain explosive regimes, the overall reaction rate increases at the fuel-lean condition.

Neglecting the small amount of branching from $H + O_2 = OH + O$, the only chain sequence which

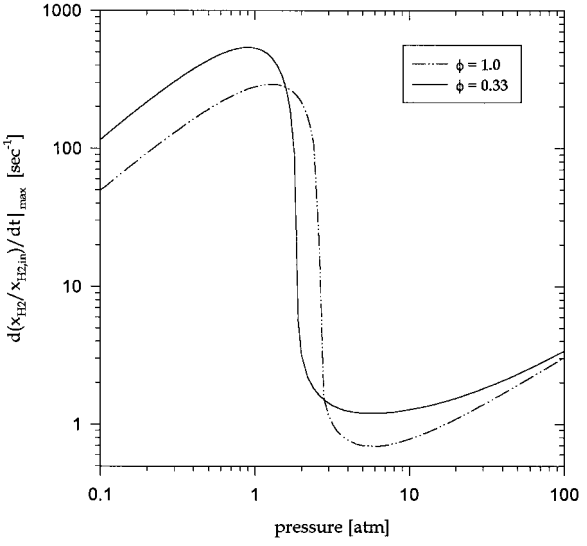

Figure 12 Maximum reaction rate as a function of pressure for stoichiometric and fuel-lean $H_2/O_2/N_2$ mixtures with reaction temperatures of 935 K. Maximum rates of reaction are determined using SENKIN [42] with constant pressure and temperature assumptions. Initial mole fractions are 1.0% H_2, 0.5% O_2, and 98.5% N_2 for $\varphi = 1$ and 1.0% H_2, 1.5% O_2, and 97.5% N_2 for $\varphi = 0.33$.

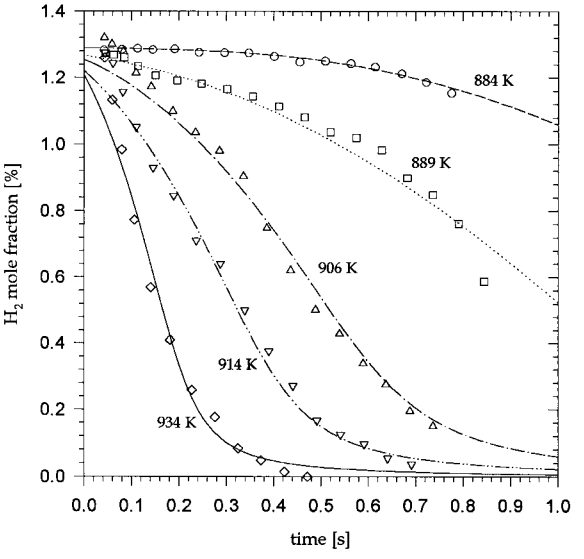

Figure 13 Reaction profiles of lean ($\varphi \approx 0.3$) $H_2/O_2/N_2$ mixtures at 6.5 atm and varying initial temperatures. Symbols represent experimental data; lines represent model predictions. Initial mole fractions are listed in the Appendix.

leads to chain branching at high pressures is

$$H + O_2(+M) = HO_2(+M) \qquad (9)$$

$$HO_2 + H_2 = H_2O_2 + H \qquad (17R)$$

$$H_2O_2(+M) = OH + OH(+M). \qquad (14)$$

However, this sequence is slow relative to the straight chain sequences discussed earlier and, in the thermal/chain regime, H_2/O_2 kinetics are nearly straight-chain in nature. Figure 13 presents H_2 mole fraction profiles from a series of experiments at 6.5 atm in which the initial temperature was varied from 884 to 934 K. With the exception of the first few data points in the profiles obtained at initial temperatures above 906 K, model predictions and experimental data are in good agreement. By defining the overall reaction rate as $d[H_2]/dt = -k_{ov}[H_2][O_2]^{1/2}$ where $k_{ov} = A\exp(-E_{ov}/RT)$, these data can be used to estimate the overall activation energy in the thermal/chain explosive regime. The reaction rate data, shown in Arrhenius form in Figure 14, indicate an overall activation energy of 61 ± 10 kcal/mole which is in good agreement with a value of $E_{ov} = E_1 + E_{15} - E_{16} = 58.3$ kcal/mole calculated using a steady state analysis of reactions (1–3), (9), and (14–16) with the assumption that $k_{9,eff} \gg 2k_1$. These results support those of Baldwin and Mayer [14] who determined an activation energy of 57.0 kcal/mole for the slow reaction of H_2/O_2 mixtures in boric-acid coated vessels. When compared to the overall activation energy of approximately 16

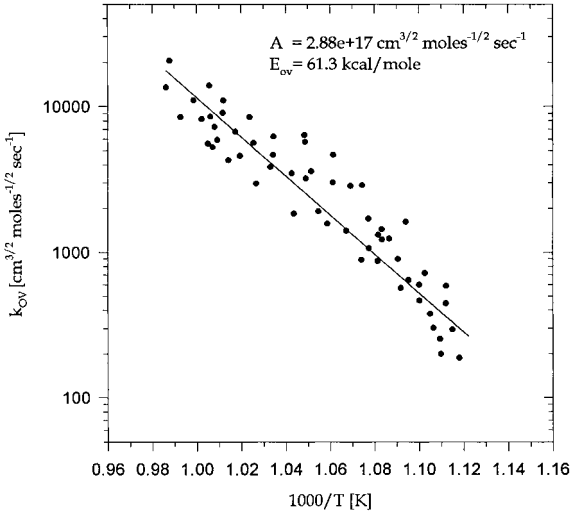

Figure 14 Arrhenius plot of overall rate constant data derived from the experimental data shown in Figure 13 except for those obtained at $T_{in} = 884$ K (for which there is a very small extent of reaction). Symbols represent experimental data; the line is a least-squares fit of the form $k_{ov} = A\exp(-E_{ov}/RT)$.

Appendix Initial Conditions for the Experimental Data Reported Here (x_{N2} = balance)

			mole fractions [%]	
Figure	P [atm]	T_{in} [K]	H_2	O_2
4	3.02	934	0.95	0.49
5(a)	2.55	935	1.01	0.52
5(b)	3.44	933	1.01	0.52
5(c)	6.00	934	1.01	0.52
8	0.30	880	0.50	0.50
10(a)	0.60	897	0.50	0.34
	0.60	896	0.50	0.76
10(b)	2.55	935	1.01	0.52
	2.50	943	1.00	1.50
10(c)	15.70	914	1.18	0.61
	15.70	914	1.18	2.21
13	6.50	884	1.29	2.19
	6.50	889	1.30	2.21
	6.50	906	1.32	2.19
	6.50	914	1.36	2.24
	6.50	934	1.36	2.24

kcal/mole in the chain explosive regime, the high overall activation energy of the H_2/O_2 reaction in the thermal/chain explosive regime underscores the importance of self-heating at conditions where $k_{9,eff} > 2k_1$.

SUMMARY AND CONCLUSIONS

Reaction profile measurements of dilute $H_2/O_2/N_2$ mixtures have been obtained at conditions ranging from 0.3 to 15.7 atm and 850–1040 K. These data, particularly those obtained at subatmospheric pressures, represent a unique contribution to the experimental data base available for the development of comprehensive reaction mechanisms. The updated H_2/O_2 mechanism provided in Tables I and II accurately predicts the experimental data over the entire range of conditions explored in this study.

New explosion limit data were also obtained for dilute $H_2/O_2/N_2$ mixtures at pressures ranging from 0.4 to 6.5 atm. The low-pressure data agree with the classical second limit criteria of $2k_1 = k_{9,eff}$, but at higher pressures where gas-phase consumption of HO_2 radicals becomes important, the data shift to an extended second limit which remains an important boundary in H_2/O_2 kinetics. In the thermal/chain explosive regime above the extended second limit, the reaction is nearly straight chain and is characterized by an overall activation energy significantly higher than in the chain explosive regime.

This work was supported by the Department of Energy, Office of Basic Energy Sciences through Grant No. DE-FG02-86ER-13503 and the Air Force Office of Scientific Research under Grant No. F49620-93-1-0427. The authors also thank Mr. Paul Michniewicz for his assistance in performing the experiments.

Author's Note: As originally referenced by Kim et al. [4], this paper was to be submitted to this journal under the authorship of T. J. Kim, R. A. Yetter, and F. L. Dryer. The current manuscript supersedes this previous reference.

REFERENCES

1. Westbrook, C. K.; Dryer, F. L. Prog Energy Combust Sci 1984, 10, 1–57.
2. von Elbe, G.; Lewis, B. Combustion, Flames, and Explosions of Gases, 3rd ed; Academic: Orlando, FL, 1987.
3. Dixon-Lewis, G.; Williams, D. J. In Comprehensive Chemical Kinetics; Bamford, C. H.; Tipper, C.F.H., Eds.; Elsevier Scientific: Amsterdam, 1977.
4. Kim, T. J.; Yetter, R. A.; Dryer, F. L. Twenty-Fifth Symposium (International) on Combustion; The Combustion Institute: Pittsburgh, PA, 1994; pp 759–766.
5. Kim, T. J. MSE Thesis, Department of Mechanical and Aerospace Engineering, Princeton University, Princeton, NJ, 1994.
6. Bromly, J. H.; Barnes, F. J.; Nelson, P. F.; Haynes, B. S. Int J Chem Kinet 1995, 27, 1165–1178.
7. Davidson, D. F.; Peterson, E. L.; Röhrig, M.; Hansen, R. K.; Bowman, C. T. Twenty-Sixth Symposium (International) on Combustion; The Combustion Institute: Pittsburgh, PA, 1996; pp 481–488.
8. Hippler, H.; Neunaber, H.; Troe, J. J Chem Phys 1995, 103, 3510–3516.
9. Mueller, M. A.; Yetter, R. A.; Dryer, F. L. Presented at the Twenty-Seventh Symposium (International) on Combustion, The Combustion Institute, Pittsburgh, PA, 1998.
10. Mueller, M. A.; Yetter, R. A.; Dryer, F. L., work in progress.
11. Allen, M. T.; Yetter, R. A.; Dryer, F. L. Combust. Flame 1998, 112, 302–311.
12. Gatto, J. L. MSE Thesis, Department of Mechanical and Aerospace Engineering, Princeton University, Princeton, NJ, 1997.
13. Yetter, R. A.; Dryer, F. L.; Rabitz, H. Combust Sci and Tech 1991, 79, 97–128.
14. Baldwin, R. R.; Mayor, L. Trans Faraday Soc 1960, 56, 80–92.
15. Baldwin, R. R.; Mayor, L.; Doran, P. Trans Faraday Soc 1960, 56, 93–102.
16. Baldwin, R. R.; Mayor, L. Trans Faraday Soc 1960, 56, 103–114.
17. Baldwin, R. R.; Jackson, D.; Walker, R. W.; Webster, S. J. Trans Faraday Soc 1967, 63, 1676–1686.

18. Baldwin, R. R.; Fuller, M. E.; Hillman, J. S.; Jackson, D.; Walker, R. W. Trans Faraday Soc 1974, 70, 635–641.
19. Kee, R. J.; Rupley, F. M.; Miller, J. A. Sandia National Laboratories Report No. SAND87-8215, 1987.
20. Hills, A. J.; Howard, C. J. J Chem Phys 1984, 81, 4458–4465.
21. Yetter, R. A.; Dryer, F. L.; Rabitz, H. Combust Sci and Tech 1991, 79, 129–140.
22. Cobos, C. J.; Hippler, H.; Troe, J. J Phys Chem 1985, 89, 342–349.
23. Slack, M. W. Combust. Flame 1977, 28, 241–249.
24. Gilbert, R. G.; Luther, K.; Troe, J. Ber Bunsenges Phys Chem 1983, 87, 169–177.
25. Pirraglia, A. N.; Michael, J. V.; Sutherland, J. W.; Klemm, R. B. J Phys Chem 1989, 93, 282–291.
26. Masten, D. A.; Hanson, R. K.; Bowman, C. T. J Phys Chem 1990, 94, 7119–7128.
27. Du, H.; Hessler, J. P. J Chem Phys 1992, 96, 1077–1092.
28. Yang, H.; Gardiner, W. C.; Shin, K. S.; Fujii, N. Chem Phys Lett 1994, 231, 449–453.
29. Ryu, S.-O.; Hwang, S. N.; Rabinowitz, M. J. J Phys Chem 1995, 99, 13984–13991.
30. Baulch, D. L.; Cobos, C. J.; Cox, R. A.; Frank, P.; Hayman, G.; Just, Th.; Kerr, J. A.; Murrells, T.; Pilling, M. J.; Troe, J.; Walker, R. W.; Warnatz, J. J Phys Chem Ref Data 1994, 23, 847–1033.
31. Keyser, L. F. J Phys Chem 1988, 92, 1193–1200.
32. Sirdharan, U. C.; Qiu, L. X.; Kaufman, F. J Phys Chem 1984, 88, 1281–1282.
33. Lii, R. R.; Gorse, R. A.; Sauer, M. C.; Gordon, S. J Phys Chem 1980, 84, 819–821.
34. Hippler, H.; Troe, J. Chem Phys Lett 1992, 192(4), 333–337.
35. Hippler, H.; Neunaber, H.; Troe, J. J Chem Phys 1995, 103, 3510–3516.
36. Keyser, L. F. J Phys Chem 1986, 90, 2994–3003.
37. Sridharan, U. C.; Qiu, L. X.; Kaufman, F. J Phys Chem 1982, 86, 4569–4574.
38. Day, M. J.; Thompson, K.; Dixon-Lewis, G. Fourteenth Symposium (International) on Combustion; The Combustion Institute: Pittsburgh, PA, 1972; pp 47–59.
39. Tsang, W.; Hampson, R. F. J Phys Chem Ref Data 1986, 15, 1087–1279.
40. Hippler, H.; Troe, J.; Willner, J. J Chem Phys 1990, 93, 1755–1760.
41. Held, T. J. Ph.D. Thesis, Department of Mechanical and Aerospace Engineering, Princeton University, Princeton, NJ, 1993.
42. Lutz, A. E.; Kee, R. J.; Miller, J. A. Sandia National Laboratories Report No. SAND87-8248, 1987.
43. von Elbe, G.; Lewis, B. J Chem Phys 1942, 10, 366–393.
44. Egerton, A.; Warren, D. R. Proc Roy Soc 1950, A 204, 465–476.
45. Baulch, D. L.; Griffiths, J. F.; Pappin, A. J.; Sykes, A. F. Combust Flame 1988, 73, 163–185.
46. Heiple, R.; Lewis, B. J Chem Phys 1941, 9, 584–590.
47. Foo, K. K.; Yang, C. H. Combust Flame 1971, 17, 223–235.
48. Kordylewski, W.; Scott, S.K. Combust Flame 1984, 57, 127–139.
49. Maas, U.; Warnatz, J. Combust Flame 1988, 74, 53–69.
50. Kreutz, T. G.; Law, C. K. Combust Flame 1998, 114, 436–456.
51. Friswell, N. J.; Sutton, M. M. Chem Phys Lett 1972, 15(1), 108–112.
52. DeMore, W. B. J Phys Chem 1982, 86, 121–126.
53. Peters, J.; Mahnen, G. Fourteenth Symposium (International) on Combustion; The Combustion Institute, Pittsburgh, PA, 1972; pp 133–146.
54. Goodings, J. M.; Hayhurst, A. N. J Chem Soc, Faraday Trans 2 1988, 84, 745–762.
55. Sutherland, J. W.; Michael, J. V.; Pirraglia, A. N.; Nesbitt, F. L.; Klemm, R. B. Twenty-First Symposium (International) on Combustion; The Combustion Institute, Pittsburgh, PA, 1986; pp 929–941.
56. Michael, J. V.; Sutherland, J. W. J Phys Chem 1988, 92, 3853–3857.
57. Sutherland, J. W.; Patterson, P. M.; Klemm, R. B. Twenty-Third Symposium (International) on Combustion; The Combustion Institute, Pittsburgh, PA, 1990; pp 51–57.
58. Warnatz, J. In Combustion Chemistry; Gardiner, W. C., Ed.; Springer-Verlag: New York, NY, 1985.
59. Brouwer, L.; Cobos, C. J.; Troe, J.; Dubal, H. R.; Crim, F. F. J Chem Phys 1985, 86, 6171–6182.
60. Baulch, D. L.; Drysdale, D. D.; Horne, D. G.; Lloyd, A. C. Evaluated Kinetic Data for High Temperature Reactions, Vols. 1 and 2; Butterworths, London, 1973.